HHS Public Access

Author manuscript

Nat Neurosci. Author manuscript; available in PMC 2012 September 01.

Published in final edited form as:

Nat Neurosci. ; 15(3): 389–S2. doi:10.1038/nn.3040.

Selective control of inhibitory synapse development by Slitrk3-PTPδ trans-synaptic interaction

Hideto Takahashi[1], **Kei-ichi Katayama**[2], **Kazuhiro Sohya**[3,4], **Hiroyuki Miyamoto**[4,5], **Tuhina Prasad**[1], **Yoshifumi Matsumoto**[2], **Maya Ota**[2], **Hiroki Yasuda**[6], **Tadaharu Tsumoto**[3], **Jun Aruga**[2,*], and **Ann Marie Craig**[1,*]

[1]Brain Research Centre and Department of Psychiatry, University of British Columbia, Vancouver, British Columbia, Canada

[2]Laboratory for Behavioral and Developmental Disorders, RIKEN Brain Science Institute (BSI), Wako-shi, Japan

[3]Laboratory for Cortical Circuit Plasticity, RIKEN BSI, Wako-shi, Japan

[4]Precursory Research for Embryonic Science and Technology (PRESTO), Japan Science and Technology Agency (JST), Saitama 332–0012, Japan

[5]Laboratory for Neurobiology of Synapse, RIKEN BSI, Wako-shi, Japan

[6]Education and Research Support Center, Gunma University Graduate School of Medicine, Maebashi, Japan

Abstract

Balanced development of excitatory and inhibitory synapses is required for normal brain function, and their imbalance may underlie pathogenesis of neuropsychiatric disorders. Compared with many identified trans-synaptic adhesion complexes that organize excitatory synapses, little is known about organizers specific for inhibitory synapses. Here we report Slit and NTRK-like family member 3 (Slitrk3) as a postsynaptic adhesion molecule that selectively regulates inhibitory synapse development via trans-interaction with axonal tyrosine phosphatase receptor PTPδ. Slitrk3 expressed in fibroblasts triggers only inhibitory presynaptic differentiation in contacting axons of cocultured rat hippocampal neurons. Recombinant Slitrk3 preferentially localizes to inhibitory postsynaptic sites. *Slitrk3*-deficient mice exhibit decreases in inhibitory but not excitatory synapse number and function in hippocampal CA1 neurons and exhibit increased seizure susceptibility and spontaneous epileptiform activity. Slitrk3 requires trans-interaction with

*Correspondence: acraig@mail.ubc.ca, jaruga@brain.riken.jp.

Contact Information:

Ann Marie Craig, Brain Research Centre Room F149, University of British Columbia, 2211 Wesbrook Mall, Vancouver, BC, Canada V6T 2B5, acraig@mail.ubc.ca, Tel 604–822–7283; FAX 604–822–7299

AUTHOR CONTRIBUTIONS

H.T. performed all the experiments involving coculture, neuron culture localization, RNAi knockdown, and protein binding assays, K.K. and J.A. performed the mouse gene targeting, K.S. and H.Y. performed the electrophysiological experiments and analysis, H.M. performed the EEG experiments, M.O., T.P. and H.T. performed the mouse immunofluorescence analysis, and Y.M. performed the mouse Western blot analysis. A.M.C., J.A. and T.T. supervised the project. H.T. and A.M.C. conceived the project and prepared the manuscript with critical input from J.A.

axonal PTPδ to induce inhibitory presynaptic differentiation. These results identify Slitrk3-PTPδ as an inhibitory-specific trans-synaptic organizing complex required for normal functional GABAergic synapse development.

INTRODUCTION

In the mature central nervous system, neurons receive inhibitory synaptic inputs from GABAergic interneurons as well as excitatory inputs from glutamatergic neurons. GABA-mediated synaptic transmission regulates neural network development and controls neuronal integration[1–3]. A proper balance between excitatory and inhibitory synapses is crucial for the normal function of networks for sensory information and cognitive processing[4,5]. Neuropsychiatric disorders such as autism, schizophrenia and Tourette's syndrome as well as neurological disorders such as epilepsy are accompanied by an imbalance between excitatory and inhibitory synapses, an imbalance thought to be a fundamental etiology of these disorders[5–9]. Thus, it is important to understand the molecular mechanisms underlying the development of GABAergic inhibitory synapses as well as glutamatergic excitatory synapses.

Key steps for synapse development include physical contact between axons and dendrites and local recruitment of presynaptic vesicles and release machinery and postsynaptic receptors and associated scaffolding and signaling proteins[10–12]. Multiple trans-synaptic organizing complexes that both mediate axon-dendrite adhesion and trigger local pre- and postsynaptic assembly have been identified for excitatory synapses, including Neuroligin1-neurexinβ[13–15], LRRTMs-neurexins[16–19], netrin G ligand 3 (NGL-3)-LAR[20], EphB-ephrinB[11], and TrkC-PTPσ[21]. Much less is known about trans-synaptic organizing complexes for inhibitory synapses. Postsynaptic neuroligin-2 complexes with presynaptic neurexins at inhibitory synapses[13,22], yet mice lacking neuroligin-2 exhibit normal numbers of inhibitory synapses and relatively subtle functional defects[23–25], suggesting the existence of unknown inhibitory synaptic organizing proteins.

We recently isolated Slit and NTRK-like family member 2 (Slitrk2) as a transmembrane protein that triggers presynaptic differentiation, through a neuron-fibroblast co-culture screen combined with bioinformatics[18]. The Slitrk family has six isoforms, and all isoforms have extracellular leucine-rich repeat domains[26], a typical synaptogenic cell adhesion domain. Interestingly, *Slitrk1* variants are associated with Tourette's syndrome[27] and Trichotillomania[28], obsessive compulsive disorders (OCDs), and *Slitrk2* is a candidate gene for schizophrenia[29] and bipolar disorder[30]. Further, *Slitrk1*-deficient mice show elevated anxiety-like behavior[31] and *Slitrk5*-deficient mice show OCD-like behaviors[32]. Despite these strong associations of *Slitrks* with multiple psychiatric disorders and behavioral abnormalities, little is reported about their cellular function other than ability to alter neurite outgrowth[26]. Based on the synaptogenic activity of Slitrk2, extracellular domain structure of the Slitrks, and the linkage of *Slitrk* genes with neuropsychiatric disorders, we hypothesize that Slitrks control synaptic development and function.

In this study, using a neuron-fibroblast coculture assay for all Slitrks, we identify Slitrk3 as uniquely able to induce inhibitory and not excitatory presynaptic differentiation.

Furthermore, we identify tyrosine phosphatase receptor PTPδ as the functional presynaptic receptor for Slitrk3. Extensive induction, localization, and loss-of function experiments *in vitro* and *in vivo* support the selective control of functional inhibitory synapse development by Slitrk3.

RESULTS

Slitrk3 induces inhibitory presynaptic differentiation

We recently reported that Slitrk2, one of six Slitrk family members, has activity to induce presynaptic differentiation in neuron-fibroblast coculture[18]. Thus, we first tested here whether all members of the Slitrk family induce presynaptic differentiation. To address whether each Slitrk induces both excitatory and inhibitory presynaptic differentiation, we quantified the clustering of inhibitory presynaptic marker vesicular GABA transporter VGAT and excitatory presynaptic marker vesicular glutamate transporter VGLUT1 on axons contacting COS cells expressing each extracellular HA-tagged Slitrk (Fig. 1a–d). All Slitrk family members have synaptogenic activity compared with negative control CD4 (Fig. 1d). Slitrk2 induced the clustering of both VGAT and VGLUT1 as efficiently as positive-control neuroligin-2, the most potent of the neuroligins (Fig. 1b,d). Interestingly, unlike any other known synaptogenic adhesion molecule, Slitrk3 induced only clustering of VGAT but not of VGLUT1 in coculture (Fig. 1a,d). This result suggests that Slitrk3 may function specifically at inhibitory synapses.

All Slitrks increased axon adhesion to COS cells, although the < 3-fold increase in axon adhesion (Supplementary Fig. 1) was not sufficient to account for the large increase in presynaptic differentiation (Fig. 1d, data already normalized per axon contact area). The effect of Slitrk3 on axon adhesion was weaker than that of the other Slitrks, in spite of good cell surface expression (Supplementary Fig. 1). Considering that > 90% of the neurons and thus axons in these cultures are glutamatergic[33], this finding is consistent with the idea that Slitrk3 may mediate adhesion only to GABAergic axons.

Slitrk3 also induced the clustering of the GABA synthetic enzyme glutamic acid decarboxylase GAD65 (Supplementary Fig. 1), the vesicle protein synaptophysin and the active zone protein bassoon (data not shown). Further, Slitrk3 induced uptake of antibodies against the luminal domains of VGAT (Fig. 1e,f) and of synaptotagmin I (SynTag) (Fig. 1f and Supplementary Fig. 1), which are accessible on the neuron surface only during active recycling of synaptic vesicles. Together, these data indicate that Slitrk3 selectively induces the differentiation of functional inhibitory presynaptic terminals.

Slitrk3 localizes to inhibitory postsynaptic sites

We next investigated the subcellular localization of Slitrk3. Because of the lack of Slitrk3 antibody available for immunocytochemistry, we determined the localization of extracellular YFP-tagged Slitrk3 in transfected cultured hippocampal neurons with low-level expression (Fig. 2). The expression of YFP-Slitrk3 for the localization analysis did not change inhibitory or excitatory synapse number (Supplementary Fig. 2). Fluorescent signals from YFP-Slitrk3 were detected in a punctate pattern on dendrites at 15 days *in vitro* (DIV) (Fig.

2). A majority of YFP-Slitrk3 puncta colocalized well with clusters of the inhibitory postsynaptic scaffold gephyrin apposed to VGAT (Fig. 2a) and with GABA receptor γ2 clusters apposed to VGAT (Fig. 2b), but hardly colocalized with excitatory postsynaptic scaffold PSD-95 or VGLUT1 (Fig. 2c,d). The presence of YFP-Slitrk3 puncta in dendrites but not axons of transfected neurons indicated postsynaptic and not presynaptic accumulation (Supplementary Fig. 3).

In quantitative analysis, a majority of VGAT clusters (78.1 ± 3.1%) apposed to YFP-Slitrk3-expressing neurons overlapped with YFP-Slitrk3 puncta, whereas a minority of VGLUT1 (5.2 ± 0.8%) apposed to the same neurons overlapped with YFP-Slitrk3 clusters (Fig. 2e). Conversely, a majority of YFP-Slitrk3 clusters (84.7 ± 2.1%) overlapped with VGAT clusters, whereas a minority of YFP-Slitrk3 (6.3 ± 1.0 %) overlapped with VGLUT1 clusters (Fig. 2e,f). Further, 80.6 ± 2.1% of YFP-Slitrk3 clusters overlapped with gephyrin apposed to VGAT (Fig. 2a,f). These data support that Slitrk3 preferentially localizes to inhibitory postsynaptic sites.

Knockdown of Slitrk3 reduces inhibitory synapse number

Next, we tested whether endogenous Slitrk3 is required for inhibitory synapse development in hippocampal neurons by RNA interference. Two independent short-hairpin RNA (shRNA) constructs for knockdown of Slitrk3, sh-Slitrk3#1, sh-Slitrk3#2, reduced expression of recombinant Slitrk3 to < 17% in HEK cells and reduced levels of endogenous Slitrk3 in cultured neurons (Supplementary Fig. 4).

Knockdown of Slitrk3 in cultured hippocampal neurons by either sh-Slitrk3#1 or sh-Slitrk3#2 reduced inhibitory synapse density assessed by VGAT-positive gephyrin clusters compared with neurons transfected with control shRNA (sh-con) (Fig. 3a,b). Knockdown of Slitrk3 by the two shRNA vectors had no significant effect on density of excitatory synapses assessed by VGLUT1-positive PSD95 clusters (Fig. 3c,d). The reduction of VGAT-positive gephyrin cluster density by sh-Slitrk3#1 was fully rescued by expression of HA-Slitrk3* resistant to sh-Slitrk3#1 (Fig. 3a,b). These data indicate that endogenous Slitrk3 is required selectively for inhibitory synapse development in cultured hippocampal neurons.

Reduced inhibitory synapse density in *Slitrk3*$^{-/-}$ mice

To address the involvement of endogenous Slitrk3 in inhibitory synapse development *in vivo*, we generated *Slitrk3*-deficient (*Slitrk3*$^{-/-}$) mice by gene targeting (Fig. 4a,b). The single protein-coding exon of *Slitrk3* (exon 2) was replaced by the neo cassette. Complete loss of Slitrk3 protein was confirmed by Western blot from frontal cortex and hippocampus of adult *Slitrk3*$^{-/-}$ mice (Fig. 4c). *Slitrk3*$^{-/-}$ mice exhibited no obvious defects in gross brain morphology (Supplementary Fig. 5).

We performed immunohistochemistry for the inhibitory presynaptic marker GAD67 on sagittal brain sections from *Slitrk3*$^{-/-}$ mice (Fig. 4d). Interestingly, *Slitrk3*$^{-/-}$ mice had a marked decrease in immunoreactivity for GAD67 in the middle layer of CA1 stratum pyramidale. We further investigated inhibitory synapse number in *Slitrk3*$^{-/-}$ mice by quantifying the immunofluorescent signals of another inhibitory presynaptic marker GAD65

in coronal sections of hippocampal brain regions (Fig. 4e). Like the decrease in GAD67, GAD65 immunoreactivity was also decreased in the middle layer of CA1 stratum pyramidale in *Slitrk3*$^{-/-}$ compared to wild-type (*Slitrk3*$^{+/+}$) mice. In high magnification images, GAD65 but not VGLUT1 also appeared diminished in CA1 stratum radiatum of the hippocampus from *Slitrk3*$^{-/-}$ mice (Fig. 4f). Considering the apparently spared GAD65 at the edges of stratum pyramidale, we performed measures to determine whether there was a redistribution of GAD65-immunoreactive terminals or an overall loss. The total area of GAD65 clusters was significantly decreased overall in stratum pyramidale of *Slitrk3*$^{-/-}$ mice, selectively in the middle sub-layer of stratum pyramidale, with no change in the superficial and deep sub-layers, compared to wild-type (Fig. 4g). There was no difference between genotypes in the density of DAPI-positive nuclei (wild-type: 57.4 ± 2.4 cells per 5,000μm^2, *Slitrk3*$^{-/-}$: 58.2 ± 2.9 cells per 5,000μm^2, Mann-Whitney's *U* test, *P* =0.73). The total area of GAD65 clusters was also decreased in stratum radiatum of *Slitrk3*$^{-/-}$ mice although there was no difference in total area of VGLUT1 clusters between *Slitrk3*$^{-/-}$ and wild-type mice (Fig. 4h). Thus, there is a selective loss of GAD65 in specific hippocampal laminae. These data indicate that endogenous Slitrk3 is involved in inhibitory synapse development *in vivo*.

Reduced inhibitory transmission at *Slitrk3*$^{-/-}$ synapses

Next, we tested whether Slitrk3 is important specifically for the development of functional inhibitorysynapses *in vivo*. We performed whole-cell recordings on CA1 pyramidal neurons in acute hippocampal slices of *Slitrk3*$^{-/-}$ mice and wild-type littermates to measure spontaneous miniature inhibitory postsynaptic currents (mIPSCs) as well as spontaneous miniature excitatory postsynaptic currents (mEPSCs).

In *Slitrk3*$^{-/-}$ mice, mIPSC frequency, but not amplitude, was significantly decreased (corresponding to an increased inter-event interval) compared to wild-type mice (Fig. 5a–c). On the other hand, mEPSCs from *Slitrk3*$^{-/-}$ mice were comparable to those from wild-type mice in frequency and amplitude (Fig. 5d–f), indicating that Slitrk3 is not essential for the development of functional excitatory synapses. Together with selective reductions of inhibitory presynaptic markers in *Slitrk3*$^{-/-}$ mice (Fig. 4d–h), these data indicate that Slitrk3 plays an important role in regulating the number of functional inhibitory synapses *in vivo*.

Epileptic seizures in *Slitrk3*$^{-/-}$ mice

A reduction of functional inhibitory synapses in hippocampus may cause various neurological disorders, particularly epilepsy[9]. We therefore tested the effect of *Slitrk3* deficiency on seizure susceptibility by intraperitoneal administration of the chemoconvulsant pentylenetetrazol (PTZ, a GABA receptor antagonist, 50 mg/kg) to *Slitrk3*$^{+/+}$, *Slitrk3*$^{+/-}$ and *Slitrk3*$^{-/-}$ mice. The severity of PTZ-induced convulsive seizures was assessed by a scoring scale from 0 (no abnormal behavior) to 5 (death). PTZ-induced seizure severity was significantly increased in *Slitrk3*$^{-/-}$ mice compared to wild-type mice (Fig. 6a). Average seizure score for 4–10 min after PTZ administration was about twofold higher in *Slitrk3*$^{-/-}$ mice (3.8 ± 0.3; $P < 0.05$) and about 1.5 times higher in *Slitrk3*$^{+/-}$ mice (3.2 ± 0.6; $P > 0.05$) than in wild-type mice (2.0 ± 0.3) (Fig. 6b). These data indicate that *Slitrk3* deficiency increases seizure susceptibility in a gene dosage-dependent manner.

During routine handling, occasional spontaneous seizures were observed in *Slitrk3*$^{-/-}$mice, characterized by sudden stillness, abnormal head movement, and/or clonus of the forelimbs. Similar seizure behaviors were never observed in wild-type littermates. Therefore, we performed electroencephalogram (EEG) monitoring with simultaneous video recording to detect spontaneous seizures in *Slitrk3*$^{-/-}$ mice in the absence of convulsant (Fig. 6c–f). Epileptiform activity was never observed either electrographically or behaviorally in three wild-type mice (Fig. 6c). In contrast, EEG/video monitoring confirmed the occurrence of spontaneous electrographic epileptiform activity associated with generalized behavioral seizures in two of three *Slitrk3*$^{-/-}$ mice (Fig. 6e), and subclinical electrographical seizures in the third. Frequent interictal sharp waves were also observed in *Slitrk3*$^{-/-}$ mice (average of 88.5 waves per hour, Fig. 6f) compared with only a few sharp waves in wild-type mice (none to three per hour). Together, these data suggest that loss of Slitrk3 enhances seizure susceptibilityand can lead to spontaneous seizures as a consequence of the selective decrease in the number of functional inhibitory synapses.

Slitrk3 binds to tyrosine phosphatase receptor PTPδ

Next, we addressed the molecular mechanisms by which Slitrk3 promotes inhibitory synapse development. Slitrk3 in COS cells induces presynaptic differentiation presumably through trans-interaction with a presynaptic receptor on contacting axons. To identify the presynaptic receptor, we screened a range of candidate proteins, including neurexins, NCAM, CHL1, neurofascin, LAR, TrkB, Casprs, and Slitrks, expressed in COS cells in a binding assay using soluble purified Slitrk3 ectodomain fused to human immunoglobulin Fc region (Slitrk3-Fc) (Fig. 7a,b). Only one candidate bound Slitrk3-Fc, protein tyrosine phosphatase receptor PTPδ.

Application of increasing amounts of Slitrk3-Fc to PTPδ-expressing COS cells revealed saturable binding (Fig. 7c). According to Scatchard analysis, the apparent dissociation constant (Kd) value is 58.6 ± 7.9 nM, within the typical nanomolar range for biologically significant ligand-receptor interactions. Slitrk3-Fc still bound to PTPδ in nominally calcium-free buffer containing 10 mM EGTA, suggesting Ca^{++}-independent interaction (Supplementary Fig. 6). Next we tested whether soluble purified PTPδ ectodomain Fc fusion (PTPδ-Fc) binds to Slitrk3 and also to the other Slitrk isoforms. PTPδ-Fc bound not only to Slitrk3 but also to all other Slitrk isoforms (Fig. 7d and Supplementary Fig. 7). These data indicate high-affinity binding of the Slitrk3 extracellular region to PTPδ, and suggest that PTPδ is a candidate for the presynaptic functional receptor through which Slitrk3, and also the other Slitrk isoforms, induce inhibitory presynaptic differentiation.

Slitrk3 trans-synaptically interacts with axonal PTPδ

We next assessed subcellular localization of PTPδ. Because there is no PTPδ antibody available for immunocytochemistry, we determined the localization of extracellular YFP-tagged PTPδ in transfected cultured hippocampal neurons with low-level expression. In transfected aspiny neurons at DIV 15, fluorescent signals from YFP-PTPδ were detected in a punctate pattern on axons and in a diffuse pattern in cell soma, but were not detected in any dendritic regions (Fig. 7e,f). YFP-PTPδ puncta in axons specifically localized at the contact sites of transfected axons with dendrites of nearby untransfected neurons, coclocalized with

VGAT clusters (Fig. 7f). These data indicate that PTPδ localizes to presynaptic sites in GABAergic aspiny neurons.

We next tested whether Slitrk3 induces the clustering of axonal PTPδ with VGAT by trans-interaction. We cocultured COS cells expressing Slitrk3-CFP or Amigo-CFP with hippocampal neurons cotransfected with YFP-PTPδ and mCherry. COS cells expressing Slitrk3-CFP significantly induced clustering of YFP-PTPδ colocalized with VGAT clusters on the contacting axons of the transfected aspiny neurons (Fig. 7g; total integrated intensity of YFP-PTPδ per transfected COS cell axon contact area was 13,416 ± 2,074 au per μm^2 for Slitrk3-CFP, $n = 15$ compared to 75 ± 48 au per μm^2 for control Amigo-CFP, $n = 18$; Mann-Whitney's U test, $P < 0.0001$). These data suggest that Slitrk3 induces inhibitory presynaptic differentiation through trans-synaptic interaction with axonal PTPδ. Furthermore, we confirmed that HA-PTPδ expressed in GABAergic axons and YFP-Slitrk3 expressed in the target neuron were co-accumulated at inhibitory synaptic contact sites between the GABAergic axons and their target neuron (Supplementary Fig. 8), supporting trans-synaptic interaction between Slitrk3 and PTPδ at inhibitory synapses.

Slitrk3 induces presynaptic differentiation through PTPδ

Next, we tested whether PTPδ is required for inhibitory presynaptic differentiation induced by Slitrk3. We cocultured COS cells expressing either Slitrk3-YFP, Amigo-YFP or YFP-neuroligin-2 with hippocampal neurons transfected at high (~60%) efficiency with vectors expressing either sh-con or an shRNA construct for knockdown of PTPδ (sh-PTPδ)[34] (Fig. 8a,b). COS cells expressing Slitrk3 induced little or no VGAT clustering on contacting axons of PTPδ-knockdown neurons, although Slitrk3 induced VGAT clustering on contacting axons of control neurons expressing sh-con (Fig. 8a,c) or PTPδ scrambled shRNA (sh-scb), another negative control (Supplementary Fig. 9). In contrast, COS cells expressing YFP-neuroligin-2, which functions through presynaptic receptor neurexin, induced VGAT clustering on contacting axons of both control and PTPδ-knockdown neurons with essentially the same efficiency (Fig. 8b,c). The selective effects of PTPδ knockdown on synaptogenic activityof Slitrk3 but not of neuroligin-2 suggest that the phenotype of PTPδ knockdown is not likely due to potential off-target effects of RNA interference. Taken together, these data indicate that Slitrk3 requires trans-synaptic interaction with axonal PTPδ to induce inhibitory presynaptic differentiation.

We further tested whether Slitrk2, another representative isoform, induces the clustering of axonal PTPδ with VGAT by trans-interaction and requires PTPδ for inhibitory presynaptic differentiation. When hippocampal neurons expressing YFP-PTPδ and mCherry were cocultured with COS cells, COS cells expressing Slitrk2-CFP significantly induced clustering of YFP-PTPδ colocalized with VGAT clusters on the contacting axons (Supplementary Fig. 10). Slitrk2 induced little or no VGAT clustering on contacting axons of PTPδ-knockdown neurons, although Slitrk2 induced VGAT clustering on contacting axons of control neurons (Supplementary Fig. 11a,b). Interestingly, Slitrk2 induced VGLUT1 clustering on contacting axons of PTPδ-knockdown neurons equivalently to control (Supplementary Fig. 11c,d). These data suggest that Slitrk2 requires trans-interaction with axonal PTPδ specifically for inhibitory presynaptic differentiation, and predict the

existence of different presynaptic receptors of Slitrk2 for excitatory presynaptic differentiation.

DISCUSSION

In this study, we identified Slitrk3 as a novel synaptogenic molecule selectively responsible for inhibitory synapse development. Furthermore, we identified tyrosine phosphatase PTPδ as the high-affinity presynaptic functional receptor of Slitrk3. Slitrk3 presented to axons induced inhibitory presynaptic differentiation via trans-binding to axonal PTPδ. Recombinant Slitrk3 localized to inhibitory postsynaptic sites in hippocampal neurons, and recombinant PTPδ localized to inhibitory presynaptic sites in aspiny GABAergic hippocampal neurons. The Slitrk3-knockdown experiments in culture and the *in vivo* morphological and electrophysiological analyses of *Slitrk3*$^{-/-}$ mice reveal an involvement of endogenous Slitrk3 in regulating the number of functional inhibitory, but not excitatory, synapses. In addition, *Slitrk3* deficiency caused increased susceptibility to PTZ-induced generalized seizures, and led to occasional spontaneous behavioral and electrographical seizures. Here we propose that trans-synaptic interaction between postsynaptic Slitrk3 and presynaptic PTPδ is a unique adhesion and differentiation mechanism that selectively organizes inhibitory synapse development.

The most significant finding of this study is the identification of Slitrk3 as a postsynaptic adhesion molecule that selectively organizes inhibitory presynaptic terminals. Among many known synaptogenic adhesion molecules[10,11,13,14,16–18,20,21,35] including the neuroligin, NGL, LRRTM, EphB, SALM families and TrkC, only neuroligin-2 preferentially regulates inhibitory synapse development[25,36]. Studies of *Nlgn2*$^{-/-}$ mice suggest that neuroligin-2 controls postsynaptic function at a subset of inhibitory synapses. In cortex, response amplitude specifically from fast-spiking interneurons was reduced in the absence of neuroligin-2, with no change in unitary response frequency or density of the corresponding presynaptic terminals[24]. In the hippocampal CA1 and dentate gyrus regions, perisomatic inhibitory synapses were selectively affected, with reduced transmission and loss of postsynaptic gephyrin but maintenance of presynaptic VGAT clusters[25,37]. Here we show reduced inhibitory synaptic transmission and a major loss of GAD65 and GAD67 positive presynaptic terminals in *Slitrk3*$^{-/-}$ mice in specific hippocampal CA1 laminae including the central region of CA1 stratum pyramidale (Figs. 4 and 5). Taken together, these data suggest that at perisomatic CA1 synapses, Slitrk3 and neuroligin-2 cooperatively regulate inhibitory synapse development.

At hippocampal dendritic inhibitory synapses, whereas *Nlgn2*$^{-/-}$ neurons did not show significant defects[25,37], loss of Slitrk3 affected inhibitory synapse development. Slitrk3 knockdown in hippocampal culture diminished apposed VGAT-gephyrin clusters on dendrites (Fig. 3), and *Slitrk3*$^{-/-}$ mice exhibited reduced GAD65 clustering in CA1 stratum radiatum (Fig. 4). Thus, Slitrk3 is perhaps the best candidate to trigger the differentiation of axon-dendrite physical contact sites into an inhibitory synapse. Secreted synaptogenic factors may also cooperate at some synapses; a recent study reported that FGF7 selectively regulates inhibitory presynaptic differentiation in hippocampal CA3 but not CA1 region[38]. Further work will be required to catalog all the inhibitory synapses at which Slitrk3

functions and to understand the basis for lamina-selective effects including the sparing of inhibitory terminals at the edges of CA1 stratum pyramidale in *Slitrk3*$^{-/-}$ mice.

Data presented here indicate that PTPδ is the functional presynaptic receptor for Slitrk3 to induce inhibitory presynaptic differentiation (Figs. 7 and 8). According to our recent study[21], PTPσ is the functional presynaptic receptor for TrkC to induce only excitatory presynaptic differentiation. NGL-3, which functions specifically in excitatory synapse development[20], binds to LAR, PTPσ, and PTPδ[35]. Surprisingly, recent studies show that a mental retardation-associated protein IL1RAPL1 triggers only excitatory not inhibitory presynaptic differntiation via trans-interaction with PTPδ[39,40]. Collectively, these studies indicate the importance of the PTPδ, PTPσ, LAR family as synaptic organizing proteins but also raise puzzling questions. In particular, how can Slitrk3-PTPδ function selectively in inhibitory synaptic development and ILRAPL1-PTPδ in excitatory synaptic development? PTPδ contains 3 short alternatively spliced exons in its Ig-like domains, and splicing of these exons at the meA and meB sites controls interaction with ILRAPL1 in a complicated manner[39]. The PTPδ isoform that we used in this study contains the full meA and meB inserts, and can interact with ILRAPL1[39], indicating that at least one major isoform of PTPδ can interact with both Slitrk3 and ILRAPL1, although perhaps with different affinity. Thus, it is possible that differential splicing of PTPδ in GABAegic versus glutamatergic axons contributes to selectivity in partner binding and function, rather like splicing at the S4 site in neurexins[10,41]. It will be important to determine the neuron type-specific splicing patterns of PTPδ. Additional mechanisms for specificity may also be required, for example, glutamatergic axons may express Slitrk3 synaptogenic suppressors, or/and Slitrk3 may require an additional presynaptic co-receptor for inhibitory presynaptic differentiation.

Another important finding in this study is the role of Slitrk3 in normal functional inhibitory transmission. In *Slitrk3*$^{-/-}$ mice, mIPSC frequency but not amplitude was reduced, and mEPSCs were normal in hippocampal CA1 neurons. Together with the reduced area of immunofluorescence for GAD65, these data suggest loss of a subset of functional inhibitory synapses onto CA1 neurons. Slitrk3 is widely expressed, including by hippocampal CA3 and dentate granule cells, olfactory mitral and granular cells, cerebellar Purkinje cells and multiple cortical layers[42]. The enhanced susceptibility to generalized PTZ-induced seizure and spontaneous epileptiform activityand frequent sharp waves detected by EEG may reflect a role of Slitrk3 in development of inhibitory synapses in multiple brain regions.

Slitrk family members have differential but overlapping expression patterns in the central nervous system[42], and all Slitrk family members have synaptogenic activity with distinct properties (Fig. 1). All Slitrks can interact with PTPδ (Fig. 7d) and we suggest that this interaction mediates induction of inhibitory presynaptic differentiation, as shown here for Slitrk3 (Figs.7 and 8) and Slitrk2 (Supplementary Figs. 10 and 11). However, excitatory presynaptic induction by Slitrk2, and presumably by other Slitrks, apparently involves a distinct presynaptic binding partner, as yet unidentified. The findings that *Slitrk5*$^{-/-}$ mice have impaired corticostriatal synaptic transmission with altered postsynaptic composition of glutamate receptors[32] and *Slitrk1*$^{-/-}$ mice have elevated anxiety-like behavior[31] supports the idea that multiple Slitrk family members may participate in inhibitory and/or excitatory synapse development. *Ptprd*$^{-/-}$ mice lacking PTPδ exhibit impaired spatial learning and

enhanced long-term potentiation[43], supporting the idea that PTPδ also regulates synapse development and function, although perhaps in a complex manner.

Accumulating evidence for a role of synaptic organizing genes in cognitive disorders[41,44] along with the results presented here suggest that further assessment of *SLITRKs* and *PTPRD* in neuropsychiatric disorders may be warranted. Indeed, *PTPRD* is associated with restless legs syndrome[45], four independent deletions have been found in patients with attention-deficit hyperactivity disorder[46], and a *de novo* deletion found in a patient with autism[47]. Further, multiple reports link *SLITRK1* to obsessive compulsive disorders[27,28], and altered expression of microRNA against SLITRK3 was recently found in autistic patients[48]. In particular, considering the seizure susceptibility in *Slitrk3*$^{-/-}$ mice, resequencing of *SLITRK3* in the significant fraction of autism spectrum disorder patients with associated epilepsy may prove informative. More comprehensive behavioral and electrophysiological analyses of *Slitrk3*$^{-/-}$ and *Ptprd*$^{-/-}$ mice will also help define the precise role of this synaptic organizing complex in inhibitory synaptic transmission and cognitive function.

METHODS

DNA constructs

The full-length cDNAs for mouse Slitrk1 (clone ID: mKIAA1910), Slitrk2 (40060548), Slitrk3 (6844461), Slitrk4 (40096585), Slitrk6 (4832410J21) and human PTPδ (40027582) were purchased from Kazusa DNA Research Institute, Open Biosystems or Source BioScience imaGenes. The cDNA for full-length rat Slitrk5 (NM001107284) was cloned by RT-PCR from a P11 rat brain cDNA library[18] and subcloned into ECFP-N1. For expressing extracellular HA-tagged Slitrks, cDNA encoding the mature form of each protein was subcloned into spSLK3-HA-C1, a vector that expresses HA with an N-terminal signal sequence derived from Slitrk3. For expressing extracellular YFP-tagged Slitrk3 and PTPδ, cDNA encoding the mature form of each protein was subcloned into spYFP-C1, a vector that expresses YFP with an N-terminal signal sequence derived from the NMDA receptor NR2B[13,18,21]. For low-level expression of YFP-Slitrk3, the YFP-Slitrk3 was subcloned into LenLox3.7 variant pLL(syn)CFP, replacing CFP to express YFP-Slitrk3 under the Synapsin I promoter. For expressing Slitrk3 with a C-terminal CFP or YFP fusion, full-length Slitrk3 lacking the stop codon was subcloned into pECFP-N1 or pEYFP-N1 (Clontech). All constructs were verified by DNA sequencing.

For RNA interference, complementary oligonucleotides encoding inverted repeats that target nucleotides 439–457 (GGCTTAGAAAGTCTGGAAT) and 1953–1971 (GCCACTTTCTGTGTTGATT) of rat and mouse Slitrk3 were annealed and ligated into HpaI/XhoI sites of LenLox3.7 variants, pLL(syn)CFP or pLL(CMV)mCherry[21] to generate sh-Slitrk3#1 and sh-Slitrk3#2, respectively. The CMV promoter vectors were used to test knockdown in HEK cells while the synapsin promoter vectors were used for knockdown in neurons. For PTPδ knockdown, the targeted sequence previously verified for specific knockdown of rat PTPδ (GTGCCGGCTAGAAACTTGT)[34] was used. We used sh-MORB as control sh-RNA, which has no effects on neuronal morphology including the densities of excitatory and inhibitory synapses and dendritic spines[21]. The scrambled sequence (GTGATCATCGGAGAGTCCT) was also used as another negative control for PTPδ

knockdown. The construct for expressing HA-Slitrk3* resistant against sh-Slitrk3#1 was generated by making the following five silent point mutations in the sh-Slitrk3#1-targeting site, indicated by underlines: GGACTAGAGAGTTTGGAGT. All constructs were verified by DNA sequencing. All other constructs were previously described[18,19,21].

Generation and confirmation of Slitrk3-deficient mice

Slitrk3-null mutant mice (*Slitrk3*$^{-/-}$) were generated using methods described previously[31]. Briefly, to construct the *Slitrk3* targeting vector, a *Slitrk3*-containing BAC clone was purchased from BACPAC Resources, Children's Hospital Oakland Research Institute. The targeting construct contained the 2.2 kb 5′ and 5.3 kb 3′ homology regions, and the 3.3 kb fragment containing the open reading frame (ORF) of *Slitrk3* was replaced with a phosphoglycerol kinase (PGK)-neo expression cassette. E14 embryonic stem cells were transformed with the targeting construct by electroporation and selected with G418. Drug-resistant clones were screened by Southern blot analysis using *Sca*I-digested genomic DNA hybridized, respectively, with 5′ (0.6 kb) and 3′ (0.7 kb) genomic fragments corresponding to sequences outside of the targeting vector and a 1.1 kb ORF probe. Chimeric mice were generated by the injection of targeted embryonic stem cells into C57BL/6J blastocysts. The correct insertion of the PGK-neo cassette was confirmed by Southern blot analysis. Genotyping of progeny was performed by Southern blot or PCR analysis of genomic DNA extracted from tails. Mice for analyses were maintained on a mixed C57BL/6J-129SV background.

Cerebral cortex and hippocampus of wild-type and *Slitrk3*$^{-/-}$ mice were dissected and homogenized in RIPA buffer (50 mM Tris-HCl pH 7.8, 150 mM NaCl, 1% NP-40, 0.5% sodium deoxycholate, 0.1% SDS, 1 mM EDTA, 2 mM NaF, 1 mM Na_3VO_4 and protease inhibitor cocktail [Roche Diagnostics]). Extract (5 μg) was loaded onto a SDS-PAGE gel and electrophoresed. Western blot was performed with rabbit polyclonal anti-Slitrk3 (Santa Cruz Biotechnology) and mouse monoclonal anti–β-III tubulin (Promega) antibodies, appropriate secondary antibodies conjugated to horseradish peroxidase, and an ECL Plus kit (GE Healthcare).

All animal care and use was in accordance with the institutional guidelines and approved by the Institutional Committee on Use and Care of Animals.

Immunofluorescence of brain sections

Six-week-old *Slitrk3*$^{-/-}$ and *Slitrk3*$^{+/+}$ littermates were anesthetized and perfused transcardially with 2% paraformaldehyde in PBS, pH 7.4. The brain was removed, post-fixed for 2 h at 4 °C, cryoprotected in 30% (w/v) sucrose in PBS for 48 h at 4 °C, and frozen on dry ice. Cryostat sections (20 μm) were mounted on Superfrost Plus slides and stored at −80 °C. For quantitative GAD-65/VGLUT1/DAPI analysis, sections were incubated in blocking solution (PBS + 3% bovine serum albumin (BSA) and 5% normal goat serum) with 0.25% Triton X-100 and then overnight at 4 °C with primary antibodies. Anti-GAD65 (mouse IgG2a, 1:20, GAD-6, Developmental Studies Hybridoma Bank) and anti-VGLUT1 (rabbit, 1:1,000, Synaptic Systems (SYSY), 135 302) were used, followed by secondary antibodies Alexa488-goat anti-mouse IgG2a and Alexa568-goat anti rabbit IgG.

Immunostained slices were incubated with DAPI (100 ng/ml) in PBS for 10 min. For immunofluorescence for GAD67 (mouse IgG2a, 1:500, Millipore MAB 5406), an antigen retrieval protocol autoclaving in citrate buffer 5 min at 105 °C was performed.

Electrophysiology

Hippocampal slices were prepared from 6–10 week-old *Slitrk3*$^{+/+}$ or *Slitrk3*$^{-/-}$ mice using standard procedure[49]. Slices were incubated in a submersion-type incubation chamber for at least 2 h and then transferred to a recording chamber mounted on an upright microscope (BX61WI; Olympus) equipped with IR-DIC optics. Slices were perfused with artificial cerebrospinal fluid (at room temperature) that was bubbled continuously with 95% O_2 and 5% CO_2 and contained 119 mM NaCl, 2.5 mM KCl, 4.0 mM $CaCl_2$, 4.0 mM $MgSO_4$, 1.0 mM NaH_2PO_4, 26.2 mM $NaHCO_3$, 11 mM glucose and 1 μM TTX. Whole-cell voltage-clamp recordings were conducted from CA1 pyramidal cells with a Multiclamp 700B (Molecular Devices). Recording electrodes were filled with internal solution containing 135 mM Cs-$MeSO_4$, 10 mM Hepes, 0.2 mM EGTA, 8 mM NaCl, 4 mM Mg-ATP, and 0.3 mM Na_3GTP (pH 7.2 with CsOH, osmolality adjusted to 275–285 mOsm). mEPSCs were recorded at −70 mV in the presence of picrotoxin (100 μM) and mIPSCs were recorded at 0 mV in the presence of CNQX (10 μM) and D-APV (50 μM). Series and input resistances were monitored online throughout each experiment. Data were acquired at 2 KHz with Igor Pro software (Wavemetrics), and analyzed with MiniAnalysis software (Synaptosoft). 100–300 consecutive miniature events were collected and analyzed. All mEPSCs or mIPSCs above a threshold value (5 pA) were included in the data analysis and each event was verified visually. Experiments were carried out in a genotype-blinded manner.

Seizure susceptibility

Five mice for each genotype (postnatal day 32–38, 3 males and 2 females) were injected intraperitoneally with pentylenetetrazole (50 mg/kg, dissolved in saline) and observed for 10 min. For statistical analysis, seizures were scored at every 1 min as follows: no abnormal behavior (0), reduced motility and prostate position (1), partial clonus (2), generalized clonus including extremities (3), tonic-clonic seizure with rigid paw extension (4), and death (5).

Electroencephalography

Electroencephalography was measured essentially as described[50]. Recordings of electroencephalogram (EEG) and electromyogram (EMG) were performed with 6–10 weeks-old age and gender-matched *Slitrk3*$^{+/+}$ and *Slitrk3*$^{-/-}$ mice (n = 3, each genotype). Video monitoring was also performed simultaneously with EEG/EMG recording to review behavior status. Stainless steel screws (1.1 mm diameter) that served as EEG electrodes were implanted over the somatosensory cortex (1.5 mm lateral to midline, 1.0 mm posterior to bregma) under 1.5% halothane anesthesia with N_2O:O_2 (3:2) ventilation one week before recording. An indifferent electrode was implanted on the cerebellum (at midline, 2.0 mm posterior to lambda). EMG electrodes were placed in the cervical region of the trapezius muscle.

Cell Cultures, transfection, and immunocytochemistry

Cultures of hippocampal neurons, COS-7 cells, HEK cells, neuron-fibroblast cocultures, and immunocytochemistry were performed essentially as described[18,21]. Transfections into COS-7 cells and hippocampal neurons were done using FuGENE 6 (Roche) and the ProFection Mammalian Transfection System (Promega), respectively. Transfection into hippocampal neurons for YFP-Slitrk3 localization analysis and for PTPδ knockdown experiments was performed using the AMAXA nucleofector system (Kit: VPG-1003, Program: O-003, Lonza). The following primary antibodies were used for immunocytochemistry: anti-VGAT (1:1,000; SYSY; 131 003 or 131 004), anti-VGLUT1 (1:1,000; SYSY; 135 302 or 135 304), anti-gephyrin (IgG1; 1:1,000; mAb7a; SYSY), anti-GABA receptor γ2 (1:1,000; SYSY; 224 003), anti-PSD-95 family (IgG2a; 1:500; 6G6-1C9; Thermo Scientific; recognizes PSD-95, PSD-93, SAP102 and SAP97), anti-Tau-1 (IgG2a; 1:2,000; PC1C6; Millipore; recognizes dephosphorylated tau), anti-HA (IgG2b; 1:1,000; 12CA5; Roche). For labeling dendrites, we used anti-MAP2 (chicken polyclonal IgY; 1:8,000; Abcam; ab5392). We used highly cross-adsorbed, Alexa-dye conjugated secondary antibodies generated in goat towards the appropriate species and monoclonal isotype (1:500; Invitrogen; Alexa-488, Alexa-568, and Alexa-647). AMCA conjugated anti-chicken IgY (donkey IgG; 1:200; Jackson ImmunoResearch; 703–155–155) was used for visualizing dendrites. For the antibody uptake assay for labeling recycling synaptic vesicles, live neurons were incubated with antibodies to the VGAT luminal domain (rabbit; SYSY; 131 103) or the synaptotagmin luminal domain (IgG1; clone 604.2; SYSY) at 1:200 for 30 min in culture media at 37 °C in a 5% CO_2 incubator. For surface HA labeling, cultures were incubated live with anti-HA antibody (1:500 dilution) for 30 min in culture media on a frozen ice pack in a 5% CO_2 incubator at 37 °C.

To assess efficacy of sh-Slitrk3 transfection for knockdown of endogenous Slitrk3, hippocampal neurons were transfected by AMAXA nucleofection at plating and grown at high density directly on polylysine-coated culture dishes in Neurobasal media with B27 supplement (Invitrogen). At 14 DIV, cell lysate was collected and analysed by Western blot with rabbit anti-Slitrk3 (Santa Cruz Biotechnology) and rabbit anti-β-actin (1:2,500; abcam, ab8227) antibodies.

Production of soluble Slitrk3-Fc protein and binding assays

Based on previously described methods[21], soluble Slitrk3 ectodomain fused to Fc (Slitrk3-Fc), PTPδ ectodomain fused to Fc (PTPδ-Fc) and Fc as negative control were generated using stable cell lines of HEK-293 cells transfected with the corresponding expression vectors with Zeocin-resistant cassettes and purified from culture media. For testing binding of soluble Slitrk3-Fc, PTPδ-Fc or Fc, COS cells on coverslips were transfected with the expression vectors for candidate binding proteins and grown for 24 h. The transfected COS cells were washed with extracellular solution (ECS; containing, in mM: 168 NaCl, 2.4 KCl, 20 HEPES pH 7.4, 10 D-glucose, 2 $CaCl_2$, 1.3 $MgCl_2$) that contained 100 μg/ml BSA (ECS/BSA) and then incubated with ECS/BSA that contained 100 nM purified Fc-fusion protein for 1 h at room temperature. The cells were washed in ECS, fixed with 4% paraformaldehyde, incubated with blocking solution, and then with DyLight594–conjugated anti-human IgG (H+L) antibodies (donkey IgG; 1:400; Jackson ImmunoResearch) for

labeling of bound Fc proteins. For quantification, we measured the average intensity of bound Fc protein per COS cell area, subtracted for off-cell background.

Imaging, quantitative fluorescence and statistical analysis

For quantitative analysis, all image acquisition, analysis and quantification were performed by investigators blind to the experimental condition.

Cell culture images were acquired on a Zeiss Axioplan2 microscope with a 40× 1.3 numerical aperture (NA) oil objective or a 63× 1.4 NA oil objective and Photometrics Sensys cooled CCD camera using Metamorph imaging software (Molecular Devices) and customized filter sets. Controls lacking specific antibodies confirmed no detectable bleed-through between channels AMCA, CFP, YFP or Alexa 488 (imaged through a YFP filter set), mCherry or Alexa 568, and Alexa 647. Images were acquired as 12 bit grayscale and prepared for presentation using Adobe Photoshop. For quantification, sets of cells were stained simultaneously and imaged with identical settings.

For cocultures with HA-Slitrks, fields for imaging were chosen only by the surface HA and phase contrast channels, for the presence of HA-positive COS cells in a neurite-rich region. The fluorescent channels of presynaptic markers were thresholded and the total intensity of puncta within all regions positive for both surface HA (labeling transfected COS cells) and dephospho-tau (labeling axons) but negative for MAP2 (labeling dendrites) was measured. For cocultures with PTPδ-knockdown neurons, total intensity of VGAT puncta within all regions positive for both YFP (labeling transfected COS cells) and CFP-overlapping tau (labeling transfected axons) but negative for MAP2 was measured.

For the quantitative analysis of YFP-Slitrk3 localization, we chose one or two dendrites per YFP-Slitrk3-expressing neuron. The YFP-Slitrk3 and synaptic marker channels were separately thresholded and confirmed visually to select appropriate clusters following a minimal size cut-off. To define apposed objects, thresholded clusters from VGAT or VGLUT1 channels were dilated by 2 pixels and compared for pixel overlap with thresholded clusters from the YFP-Slitrk3 channel. YFP-Slitrk3 clusters colocalized with gephyrin apposed to VGAT correspond to the thresholded YFP-Slitrk3 clusters exhibiting pixel overlap with both thresholded gephyrin clusters and thresholded dilated VGAT clusters.

For neurons transfected with shRNA vectors, CFP-expressing neurons were chosen randomly based on health and expression level. After images were thresholded, synaptic protein puncta were delineated by the perimeter of the transfected or designated neuron. Three regions of dendrites per neuron were randomly selected and the number of synaptic protein puncta per dendrite length measured. VGAT-positive gephyrin clusters indicate the number of clusters with pixel overlap between the separately thresholded VGAT and gephyrin channels (and similarly for VGLUT1-positive PSD95 clusters).

For quantitative analysis of brain slices, single-plane images were captured on a Fluoview FV1000 confocal microscope (Olympus) with constant settings using a 60× 1.42 NA oil-immersion objective lens by sequential scan mode with 405, 488, and 543 nm lasers and custom filter sets. The images wereacquired at 12 bit grayscale, 10 μs per pixel, and 1024 ×

1024 pixels with a pixel size of 0.183 μm and optical thickness of 0.8 μm. We determined region of interest (ROI) using DAPI images. Quantification of GAD65 and VGLUT1 clustering in stratum radiatum was performed in the same ROI. GAD65 and VGLUT1 images were threshold by a constant grayscale value determined as the average of the automatically-calculated threshold level of all analyzed images and confirmed visually to select appropriate clusters following a minimal size cut-off. We quantified the total area of all GAD65 or VGLUT1 clusters in each ROI (total area per 1,000 μm^2), instead of quantifying the number of those clusters per area because many clusters partly overlapped.

Analysis was performed using Metamorph 6.1, Microsoft Excel, and GraphPad Prism 4. The majority of the data had non-normal distribution and non-equal variance, so statistical comparisons were made using Mann-Whitney's *U* test and Kruskal-Wallis one-way ANOVA with post-hoc Dunn's pairwise multiple comparison test, as indicated in the figure legends. Cumulative distribution was analyzed by Kolmogorov-Smirnov test. All data are reported as the mean ± standard error of the mean (s.e.m.) from at least two, mostly three, independent experiments and statistical significance was defined as $P< 0.05$.

Supplementary Material

Refer to Web version on PubMed Central for supplementary material.

Acknowledgments

We thank Xiling Zhou (Brain Research Centre, University of British Columbia) for excellent preparation of neuron cultures and Noriko Takashima (Lab for Behavioral and Developmental Disorders, RIKEN BSI) for technical assistance with seizure experiments. This work was supported by a NeuroDevNet Canadian Network of Centre of Excellence Opportunities Initiative Award, National Institutes of Health MH070860, Canadian Institutes of Health Research MOP-84241, and Canada Research Chair awards to A.M.C., a Japan Society for the Promotion of Science Postdoctoral Fellowship for Research Abroad and NARSAD Young Investigator Grant to H.T., and RIKEN BSI funds and a MEXT (Ministry of Education, Culture, Sports, Science, and Technology, Japan) Grant-in-Aid for Scientific Research (A) (21240031) to J.A.

References

1. Huang ZJ, Di Cristo G, Ango F. Development of GABA innervation in the cerebral and cerebellar cortices. Nat Rev Neurosci. 2007; 8:673–86. [PubMed: 17704810]
2. Akerman CJ, Cline HT. Refining the roles of GABAergic signaling during neural circuit formation. Trends Neurosci. 2007; 30:382–9. [PubMed: 17590449]
3. Hensch TK. Critical period plasticity in local cortical circuits. Nat Rev Neurosci. 2005; 6:877–88. [PubMed: 16261181]
4. Maffei A, Nelson SB, Turrigiano GG. Selective reconfiguration of layer 4 visual cortical circuitry by visual deprivation. Nat Neurosci. 2004; 7:1353–9. [PubMed: 15543139]
5. Cline H. Synaptogenesis: a balancing act between excitation and inhibition. Curr Biol. 2005; 15:R203–5. [PubMed: 15797012]
6. Rubenstein JL, Merzenich MM. Model of autism: increased ratio of excitation/inhibition in key neural systems. Genes Brain Behav. 2003; 2:255–67. [PubMed: 14606691]
7. Wassef A, Baker J, Kochan LD. GABA and schizophrenia: a review of basic science and clinical studies. J Clin Psychopharmacol. 2003; 23:601–40. [PubMed: 14624191]
8. Singer HS, Minzer K. Neurobiology of Tourette's syndrome: concepts of neuroanatomic localization and neurochemical abnormalities. Brain Dev. 2003; 25 (Suppl 1):S70–84. [PubMed: 14980376]

9. Mohler H. GABAA receptors in central nervous system disease: anxiety, epilepsy, and insomnia. J Recept Signal Transduct Res. 2006; 26:731–40. [PubMed: 17118808]
10. Siddiqui TJ, Craig AM. Synaptic organizing complexes. Curr Opin Neurobiol. 2010; 21:132–43. [PubMed: 20832286]
11. Dalva MB, McClelland AC, Kayser MS. Cell adhesion molecules: signalling functions at the synapse. Nat Rev Neurosci. 2007; 8:206–20. [PubMed: 17299456]
12. Shen K, Scheiffele P. Genetics and cell biology of building specific synaptic connectivity. Annu Rev Neurosci. 2010; 33:473–507. [PubMed: 20367446]
13. Graf ER, Zhang X, Jin SX, Linhoff MW, Craig AM. Neurexins induce differentiation of GABA and glutamate postsynaptic specializations via neuroligins. Cell. 2004; 119:1013–26. [PubMed: 15620359]
14. Scheiffele P, Fan J, Choih J, Fetter R, Serafini T. Neuroligin expressed in nonneuronal cells triggers presynaptic development in contacting axons. Cell. 2000; 101:657–69. [PubMed: 10892652]
15. Ichtchenko K, et al. Neuroligin 1: a splice site-specific ligand for beta-neurexins. Cell. 1995; 81:435–43. [PubMed: 7736595]
16. de Wit J, et al. LRRTM2 interacts with Neurexin1 and regulates excitatory synapse formation. Neuron. 2009; 64:799–806. [PubMed: 20064388]
17. Ko J, Fuccillo MV, Malenka RC, Sudhof TC. LRRTM2 functions as a neurexin ligand in promoting excitatory synapse formation. Neuron. 2009; 64:791–8. [PubMed: 20064387]
18. Linhoff MW, et al. An unbiased expression screen for synaptogenic proteins identifies the LRRTM protein family as synaptic organizers. Neuron. 2009; 61:734–49. [PubMed: 19285470]
19. Siddiqui TJ, Pancaroglu R, Kang Y, Rooyakkers A, Craig AM. LRRTMs and neuroligins bind neurexins with a differential code to cooperate in glutamate synapse development. J Neurosci. 2010; 30:7495–506. [PubMed: 20519524]
20. Woo J, et al. Trans-synaptic adhesion between NGL-3 and LAR regulates the formation of excitatory synapses. Nat Neurosci. 2009; 12:428–37. [PubMed: 19252495]
21. Takahashi H, et al. Postsynaptic TrkC and presynaptic PTPsigma function as a bidirectional excitatory synaptic organizing complex. Neuron. 2011; 69:287–303. [PubMed: 21262467]
22. Varoqueaux F, Jamain S, Brose N. Neuroligin 2 is exclusively localized to inhibitory synapses. Eur J Cell Biol. 2004; 83:449–56. [PubMed: 15540461]
23. Blundell J, et al. Increased anxiety-like behavior in mice lacking the inhibitory synapse cell adhesion molecule neuroligin 2. Genes Brain Behav. 2009; 8:114–26. [PubMed: 19016888]
24. Gibson JR, Huber KM, Sudhof TC. Neuroligin-2 deletion selectively decreases inhibitory synaptic transmission originating from fast-spiking but not from somatostatin-positive interneurons. J Neurosci. 2009; 29:13883–97. [PubMed: 19889999]
25. Poulopoulos A, et al. Neuroligin 2 drives postsynaptic assembly at perisomatic inhibitory synapses through gephyrin and collybistin. Neuron. 2009; 63:628–42. [PubMed: 19755106]
26. Aruga J, Mikoshiba K. Identification and characterization of Slitrk, a novel neuronal transmembrane protein family controlling neurite outgrowth. Mol Cell Neurosci. 2003; 24:117–29. [PubMed: 14550773]
27. Abelson JF, et al. Sequence variants in SLITRK1 are associated with Tourette's syndrome. Science. 2005; 310:317–20. [PubMed: 16224024]
28. Zuchner S, et al. SLITRK1 mutations in trichotillomania. Mol Psychiatry. 2006; 11:887–9. [PubMed: 17003809]
29. Piton A, et al. Systematic resequencing of X-chromosome synaptic genes in autism spectrum disorder and schizophrenia. Mol Psychiatry. 2010; 16:867–880. [PubMed: 20479760]
30. Smith EN, et al. Genome-wide association study of bipolar disorder in European American and African American individuals. Mol Psychiatry. 2009; 14:755–63. [PubMed: 19488044]
31. Katayama K, et al. Slitrk1-deficient mice display elevated anxiety-like behavior and noradrenergic abnormalities. Mol Psychiatry. 2010; 15:177–84. [PubMed: 18794888]

32. Shmelkov SV, et al. Slitrk5 deficiency impairs corticostriatal circuitry and leads to obsessive-compulsive-like behaviors in mice. Nat Med. 2010; 16:598–602. 1p following 602. [PubMed: 20418887]
33. Benson DL, Watkins FH, Steward O, Banker G. Characterization of GABAergic neurons in hippocampal cell cultures. J Neurocytol. 1994; 23:279–95. [PubMed: 8089704]
34. Dunah AW, et al. LAR receptor protein tyrosine phosphatases in the development and maintenance of excitatory synapses. Nat Neurosci. 2005; 8:458–67. [PubMed: 15750591]
35. Kwon SK, Woo J, Kim SY, Kim H, Kim E. Trans-synaptic adhesions between netrin-G ligand-3 (NGL-3) and receptor tyrosine phosphatases LAR, protein-tyrosine phosphatase delta (PTPdelta), and PTPsigma via specific domains regulate excitatory synapse formation. J Biol Chem. 2010; 285:13966–78. [PubMed: 20139422]
36. Chih B, Engelman H, Scheiffele P. Control of excitatory and inhibitory synapse formation by neuroligins. Science. 2005; 307:1324–8. [PubMed: 15681343]
37. Jedlicka P, et al. Increased dentate gyrus excitability in neuroligin-2-deficient mice in vivo. Cereb Cortex. 2011; 21:357–67. [PubMed: 20530218]
38. Terauchi A, et al. Distinct FGFs promote differentiation of excitatory and inhibitory synapses. Nature. 2010; 465:783–7. [PubMed: 20505669]
39. Yoshida T, et al. IL-1 Receptor Accessory Protein-Like 1 Associated with Mental Retardation and Autism Mediates Synapse Formation by Trans-Synaptic Interaction with Protein Tyrosine Phosphatase δ. J Neurosci. 2011; 31:13485–99. [PubMed: 21940441]
40. Valnegri P, et al. The X-linked intellectual disability protein IL1RAPL1 regulates excitatory synapse formation by binding PTPδ and RhoGAP2. Hum Mol Genet. 2011; 20:4797–809. [PubMed: 21926414]
41. Sudhof TC. Neuroligins and neurexins link synaptic function to cognitive disease. Nature. 2008; 455:903–11. [PubMed: 18923512]
42. Beaubien F, Cloutier JF. Differential expression of Slitrk family members in the mouse nervous system. Dev Dyn. 2009; 238:3285–96. [PubMed: 19924824]
43. Uetani N, et al. Impaired learning with enhanced hippocampal long-term potentiation in PTPdelta-deficient mice. Embo J. 2000; 19:2775–85. [PubMed: 10856223]
44. Betancur C, Sakurai T, Buxbaum JD. The emerging role of synaptic cell-adhesion pathways in the pathogenesis of autism spectrum disorders. Trends Neurosci. 2009; 32:402–12. [PubMed: 19541375]
45. Schormair B, et al. PTPRD (protein tyrosine phosphatase receptor type delta) is associated with restless legs syndrome. Nat Genet. 2008; 40:946–8. [PubMed: 18660810]
46. Elia J, et al. Rare structural variants found in attention-deficit hyperactivity disorder are preferentially associated with neurodevelopmental genes. Mol Psychiatry. 2010; 15:637–46. [PubMed: 19546859]
47. Pinto D, et al. Functional impact of global rare copy number variation in autism spectrum disorders. Nature. 2010; 466:368–372. [PubMed: 20531469]
48. Talebizadeh Z, Butler MG, Theodoro MF. Feasibility and relevance of examining lymphoblastoid cell lines to study role of microRNAs in autism. Autism Res. 2008; 1:240–50. [PubMed: 19360674]
49. Yasuda H, Barth AL, Stellwagen D, Malenka RC. A developmental switch in the signaling cascades for LTP induction. Nat Neurosci. 2003; 6:15–6. [PubMed: 12469130]
50. Suzuki T, et al. Efhc1 deficiency causes spontaneous myoclonus and increased seizure susceptibility. Hum Mol Genet. 2009; 18:1099–109. [PubMed: 19147686]

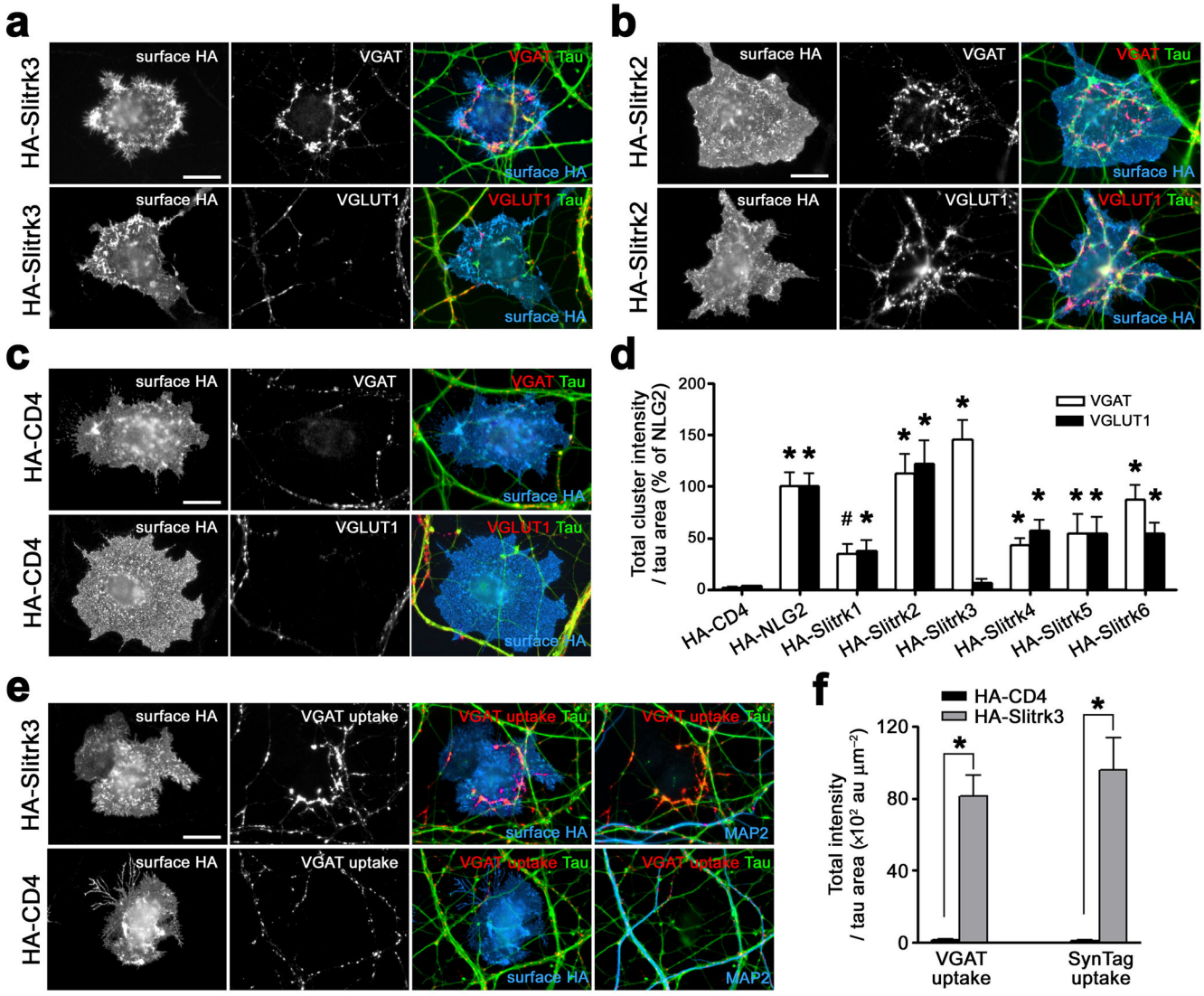

Figure 1. Slitrk3 selectively induces functional inhibitory presynaptic differentiation in coculture

(**a**) COS cells expressing HA-Slitrk3 induce clustering of VGAT but not VGLUT1 along contacting axons (labeled with dephosphorylated tau) in hippocampal neuron co-culture.

(**b**) COS cells expressing HA-Slitrk2 induce both VGAT and VGLUT1 clustering.

(**c**) COS cells expressing HA-CD4, a negative control, do not induce either VGAT or VGLUT1 clustering.

(**d**) Total integrated intensity of VGAT or VGLUT1 associated with COS cells expressing the indicated HA-tagged proteins and not associated with MAP2 (images not shown) divided by the tau-positive axon contact area, expressed as a percentage of the value for HA-neuroligin2 (HA-NLG2). Kruskal-Wallis ANOVA, $P < 0.0001$, $n \geq 30$ cells each; $*P < 0.001$, $\#P < 0.01$ compared with HA-CD4 by post-hoc Dunn's pair-wise multiple comparison test. Only HA-Slitrk3 selectively induces inhibitory presynaptic differentiation, whereas the other HA-Slitrks induce both excitatory and inhibitory presynaptic differentiation.

(**e,f**) COS cells expressing HA-Slitrk3 but not HA-CD4 induce functional inhibitory presynaptic differentiation assessed by incubating live neurons with antibodies to VGAT luminal domainor antibodies to synaptotagmin I (SynTag) luminal domain. Mann-Whitney's *U* test, **P*< 0.0001, *n* = 30 cells each.

Data are presented as mean ± s.e.m. Scale bars represent 20 μm.

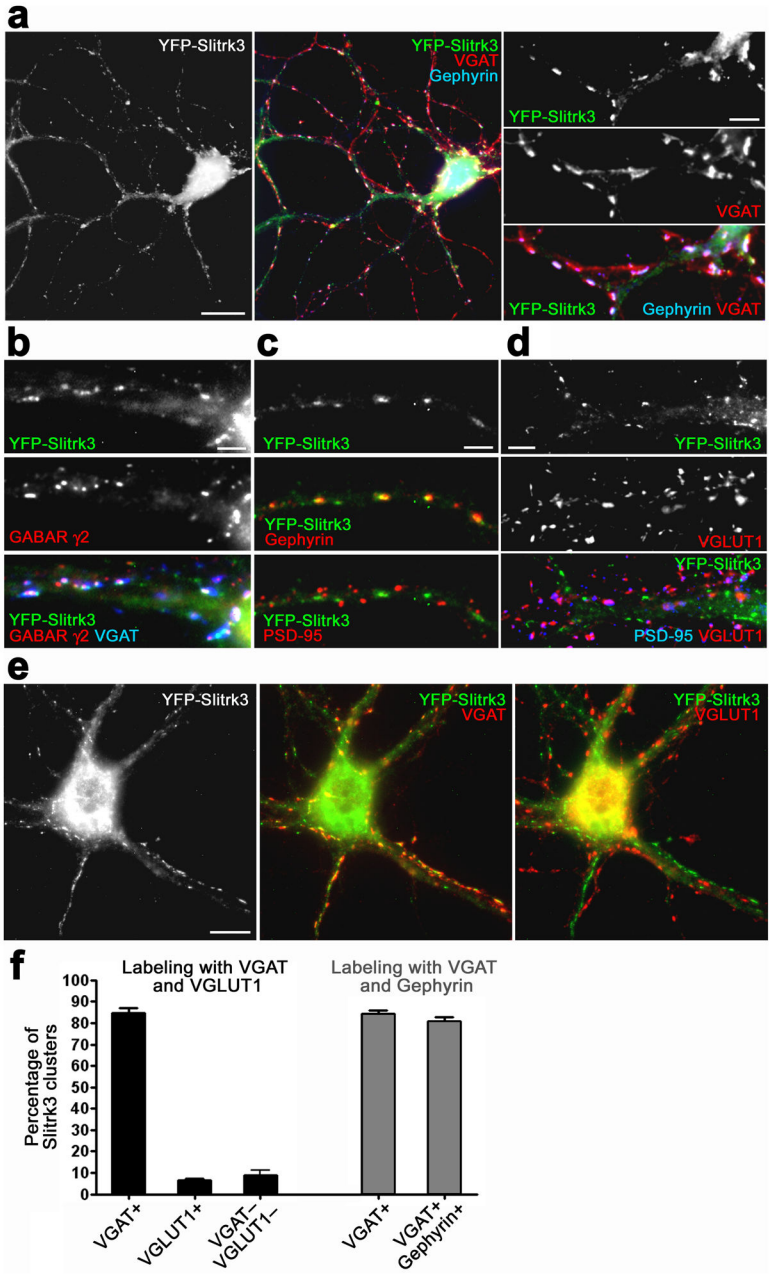

Figure 2. Recombinant Slitrk3 localizes to inhibitory postsynaptic sites

(**a, b**) Recombinant YFP-Slitrk3 expressed at low level in cultured hippocampal neurons at 15 DIV is concentrated in dendrites at GABA synapses labeled with gephyrin apposed to VGAT (**a**) or labeled with GABA receptor γ2 apposed to VGAT (**b**).

(**c, d**) YFP-Slitrk3 clusters are colocalized with gephyrin at GABA synapses (**c**, middle), but are not detected with PSD-95 (**c**, bottom) or with PSD-95 apposed to VGLUT1 at glutamate synapses (**d**).

(**e**) Double immunolabeling of YFP-Slitrk3-expressing neurons with VGAT and VGLUT1.

(**f**) Quantification of the percentage of YFP-Slitrk3 clusters apposed to VGAT clusters or to VGLUT1 clusters or not associated with either VGAT or VGLUT1 clusters, based on

double labeling with VGAT and VGLUT1 (black bars, Kruskal-Wallis ANOVA, $P < 0.0001$, $n = 30$ cells). Gray bars indicate the percentage of YFP-Slitrk3 clusters apposed to VGAT or colocalized with gephyrin apposed to VGAT, based on double labeling with VGAT and gephyrin ($n = 30$ cells).

Data are presented as mean ± s.e.m. Scale bars represent 20μm (**a**, left) 10 μm (**e**), 5 μm (**a**, right and **d**) and 3μm (**b, c**).

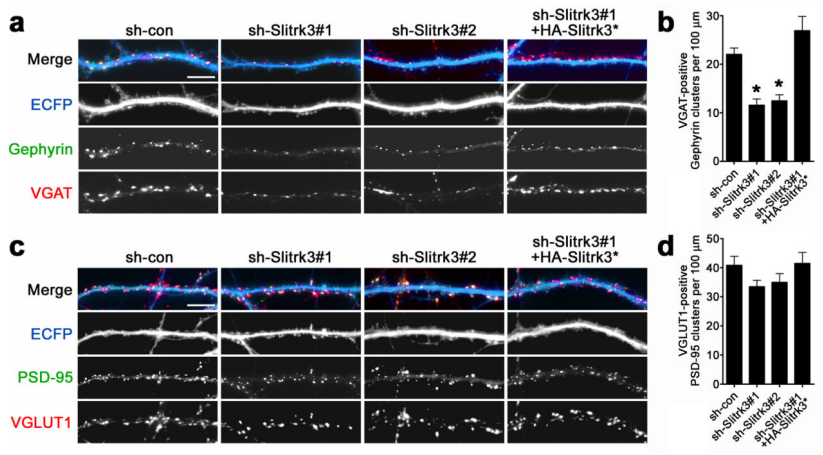

Figure 3. Slitrk3 knockdown decreases the density of inhibitory synapses in hippocampal culture

Cultured hippocampal neurons were transfected at 9–10 DIV with a vector co-expressing ECFP and either control shRNA (sh-con) or independent shRNA sequences effective to knock down Slitrk3 (sh-Slitrk3#1 and sh-Slitrk3#2). Neurons were analyzed at 15–16 DIV. Slitrk3 knockdown reduced the clusters of apposed gephyrin/VGAT marking inhibitory synapses (**a,b**) but had no effect on apposed PSD-95/VGLUT1 marking excitatory synapses (**c,d**). Co-expression of RNAi-resistant HA-Slitrk3 (HA-Slitrk3*) completely rescued the effects of Slitrk3 knockdown on inhibitory synapse markers. Kruskal-Wallis ANOVA, $P < 0.0001$ for VGAT-positive gephyrin and $P = 0.18$ for VGLUT1-positive PSD95, $n > 30$ cells each except sh-Slitrk3#1+HA-Slitrk3* $n = 20$, $^{*}P < 0.001$ compared with sh-con by Dunn's pairwise post-hoc test.

Data are presented as mean ± s.e.m. Scale bars represent 10 µm.

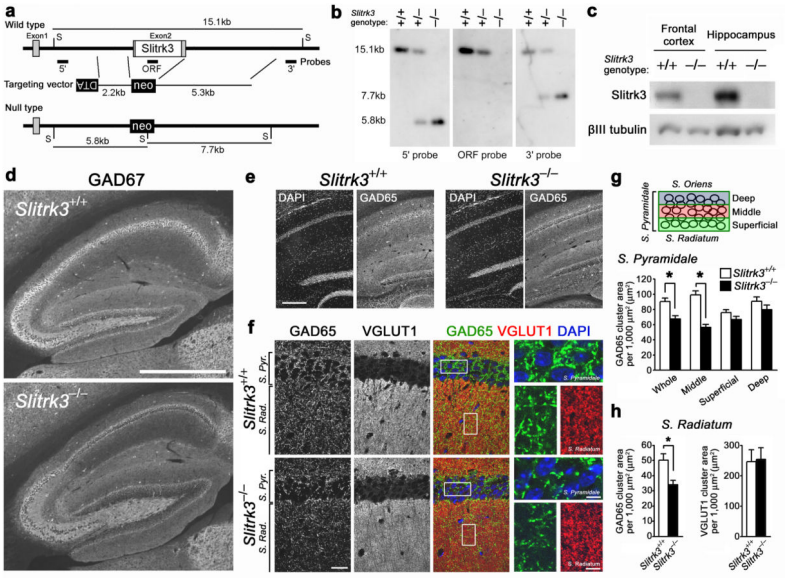

Figure 4. *Slitrk3*$^{-/-}$ mice have reduced inhibitory synapse density in CA1 region of hippocampus

(**a, b**) Strategy for targeted deletion of *Slitrk3*, and confirmation of homologous recombination by Southern blot. The entire protein-coding region (white box) in exon 2 was replaced with the PGK-neo (neo) cassette. DTA, diphtheria toxin-A cassette; gray boxes, untranslated exon regions; S, ScaI site.

(**c**) Western blot of the frontal cortex and hippocampus of adult *Slitrk3*$^{+/+}$ and *Slitrk3*$^{-/-}$mice.

(**d,e**) Immunofluorescence for inhibitory presynaptic markers GAD67 in sagittal sections (**d**) and GAD65 in coronal sections (**e**; DAPI for nuclei) from wild-type (*Slitrk3*$^{+/+}$) and *Slitrk3*$^{-/-}$ mice. Note a marked decrease in GAD67 and GAD65 immunoreactivities in the middle layer of CA1 stratum pyramidale in *Slitrk3*$^{-/-}$ mice.

(**f**) High magnification images from wild-type and *Slitrk3*$^{-/-}$ mice immunolabed for GAD65 and VGLUT1 with DAPI staining.

(**g**) For measurement, stratum pyramidale was divided into three approximately equal sub-layers based on DAPI images. Total area of clustered GAD65 was decreased in stratum pyramidale of *Slitrk3*$^{-/-}$ mice, selectively in its middle layer. Kruskal-Wallis ANOVA, $P < 0.0001$, $^{*}P < 0.001$ compared with wild-type by Dunn's pairwise post-hoc test, wild-type: $n = 59$ images from 4 mice, *Slitrk3*$^{-/-}$: $n = 83$ images from 5 mice.

(**h**) Total area of GAD65 clusters, but not VGLUT1 clusters, was decreased in stratum radiatum of *Slitrk3*$^{-/-}$ mice. Mann-Whitney's *U* test, $^{*}P < 0.001$ for GAD65 and $P = 0.38$ for VGLUT1, *n* as in (**g**).

Data are presented as mean ± s.e.m. Scale bars represent 500 μm (**d**), 200 μm (**e**), 20 μm (**f**, left) and 5 μm (**f**, right).

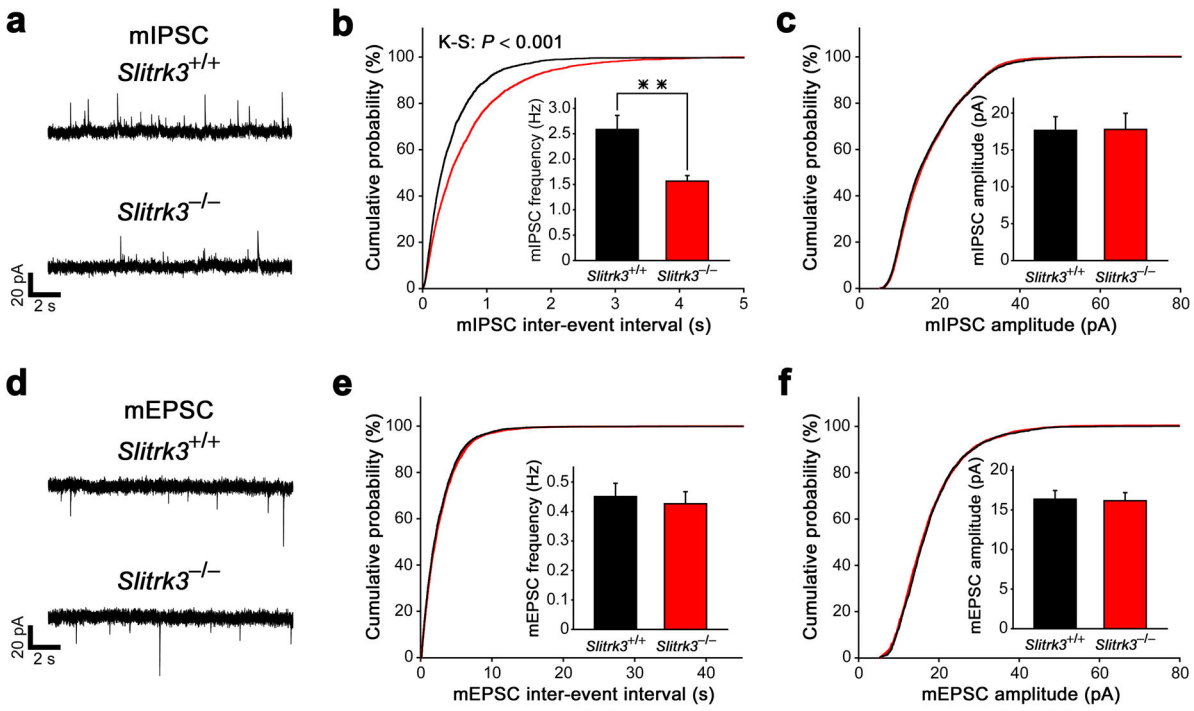

Figure 5. *Slitrk3*$^{-/-}$ mice have reduced inhibitory synaptic transmission in CA1 of the hippocampus

(**a**) Representative recordings of mIPSCs from wild-type (*Slitrk3*$^{+/+}$) and *Slitrk3*$^{-/-}$hippocampal CA1 pyramidal neurons.

(**b, c**) Cumulative distributions of mIPSC inter-event intervals (**b**) and amplitudes (**c**) in wild-type and *Slitrk3*$^{-/-}$ neurons. Insets in (**b**) and (**c**) display the mean ± s.e.m. frequency and amplitude, respectively. Kolmogorov-Smirnov (K-S) test: $P < 0.001$ for frequency and $P = 0.11$ for amplitude, Mann-Whitney's *U* test: $^{**}P < 0.001$ for frequency and $P = 0.75$ for amplitude, $n = 11$ neurons from five mice for wild-type and $n = 13$ neurons from four mice for *Slitrk3*$^{-/-}$.

(**d**) Representative recordings of mEPSCs from wild-type and *Slitrk3*$^{-/-}$ hippocampal CA1 pyramidal neurons.

(**e, f**) Cumulative distributions of mEPSC inter-event intervals (**e**) and amplitudes (**f**) in wild-type and *Slitrk3*$^{-/-}$ neurons. Insets in (**e**) and (**f**) display the mean ± s.e.m. frequency and amplitude, respectively. Kolmogorov-Smirnov test: $P = 0.09$ for frequency and $P = 0.25$ for amplitude, Mann-Whitney's *U* test: $P = 0.62$ for frequency and $P = 0.78$ for amplitude, $n = 10$ neurons from four mice for wild-type and $n = 11$ neurons from five mice for *Slitrk3*$^{-/-}$.

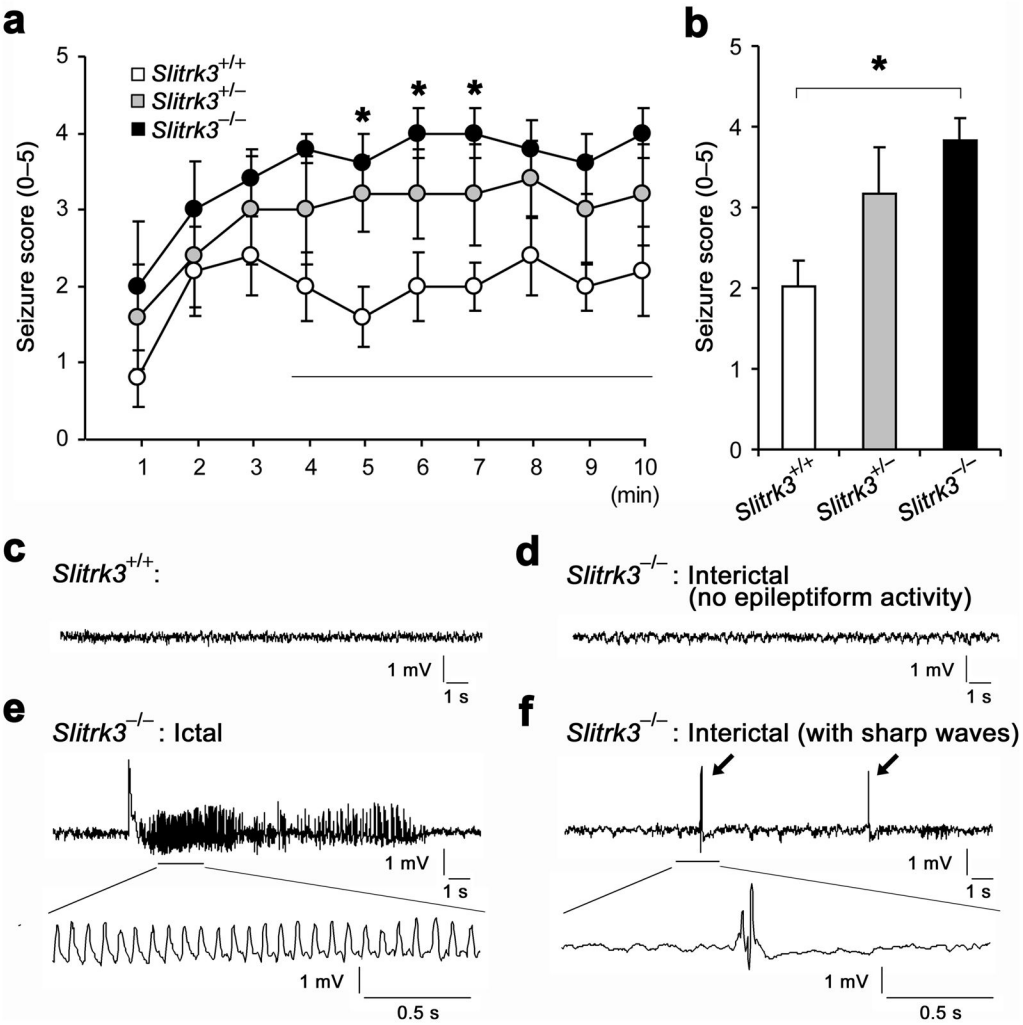

Figure 6. *Slitrk3*$^{-/-}$ mice exhibit increased seizure susceptibility and abnormal epileptiform activities in EEG recording

(**a**) Time course of mean scores of seizures induced by intraperitoneal injection of pentylenetetrazole (PTZ, 50 mg/kg) into *Slitrk3*$^{+/+}$, *Slitrk3*$^{+//-}$, and *Slitrk3*$^{-/-}$ mice (n = 5 each genotype). Seizures were scored at every 1 min for 10 min according to the following criteria: no abnormal behavior (0), reduced motility and prostate position (1), partial clonus (2), generalized clonus including extremities (3), tonic-clonic seizure with rigid paw extension (4), and death (5). Kruskal-Wallis ANOVA $P < 0.05$, *$P < 0.05$ compared with wild-type by Dunn's pairwise post-hoc test.

(**b**) Quantification of mean score values for 4–10 min in each genotype. Kruskal-Wallis ANOVA, $P = 0.021$, *$P < 0.05$ compared with wild-type by Dunn's pairwise post-hoc test, n = 5 each genotype.

(**c–f**) Representative EEG recordings under drug-free conditions from a wild-type littermate (**c**), from *Slitrk3*$^{-/-}$ micecuring an interictal period without epileptiform activity (**d**), during an ictal phase of generalized seizure with epileptiform activity (**e**) and during an interictal period with abnormal sharp waves (arrows; **f**). Two of three Slirk3$^{-/-}$ mice showed

generalized seizures in the first 24 h of EEG recording. Epileptic seizures were never observed either electrographically or behaviorally in the three wild-type mice monitored. All three Slirk3$^{-/-}$ mice showed many sharp waves in the EEG during interictal periods. The mean frequencies ± s.e.m. of the sharp wave events were: wild-type: 1.3 ± 0.7; Slitrk3$^{-/-}$: 60.7 ± 33.2 (17:00–19:00, light phase); wild-type: 3.7 ± 1.3; Slitrk3$^{-/-}$: 116 ± 55.8 (2:00–4:00, dark phase).

Data are presented as mean ± s.e.m.

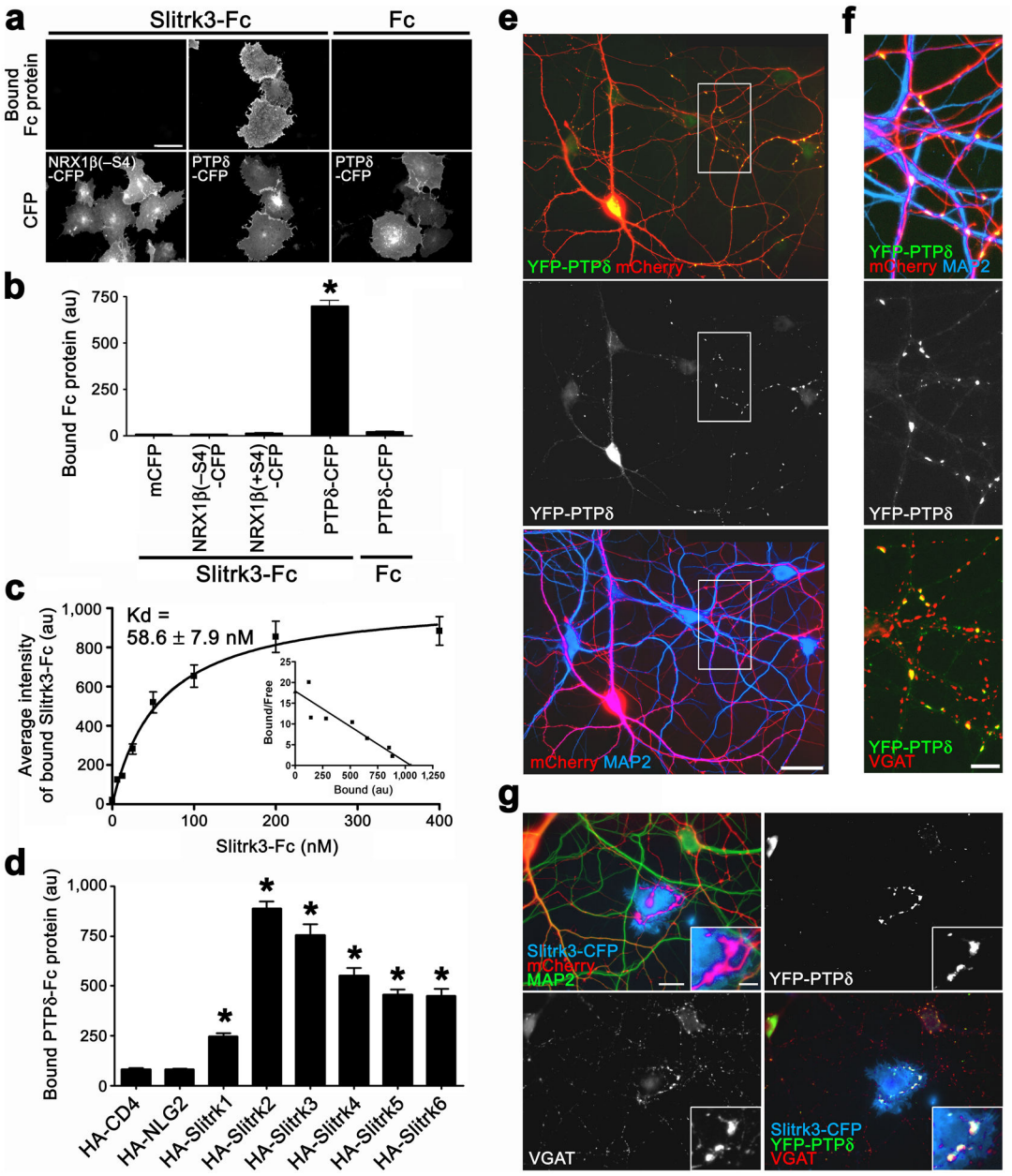

Figure 7. PTPδ is a presynaptic binding partner for Slitrk3

(**a–c**) Slitrk3-Fc proteins specifically bound to PTPδ-expressing COS cells with high affinity. Kruskal-Wallis ANOVA, $P < 0.0001$, $n > 65$ cells each; $^*P < 0.01$ compared with controls by Dunn's pairwise post-hoc test in (**b**). Scatchard analysis, $n > 25$ cells each in (**c**).

(**d**) PTPδ-Fc bound to Slitrk3 and all other Slitrk isoforms. Kruskal-Wallis ANOVA, $P < 0.0001$, $n > 45$ cells each; $^*P < 0.001$ compared with HA-CD4 by Dunn's pairwise post-hoc test.

(**e**) Cultured hippocampal neurons were co-transfected at 13 DIV with YFP-PTPδ-expressing and mCherry-expressing vectors, and immunostained with VGAT and MAP2 at 15 DIV. Axons of transfected neurons can be detected as mCherry-positive and MAP2-

negative thin protrusions. YFP-PTPδ expressed at low level in hippocampal aspiny neurons was concentrated in the soma and highly punctate in axons but hardly detected in dendrites.
(**f**) Magnified images of the boxed region in (**e**). YFP-PTPδ puncta were colocalized with VGAT clusters at presynaptic boutons where mCherry-expressing axons contact with dendrites.
(**g**) COS cells expressing Slitrk3-CFP induce YFP-PTPδ accumulation on contacting axons with VGAT. Neurons were co-tranfected with YFP-PTPδ and mCherry and then cocultured with COS cells expressing Slitrk3-CFP.
Data are presented as mean ± s.e.m. Scale bars represent 40 μm (**a, e**, **g**), 10 μm (**f**) and 5 μm (inset of **g**).

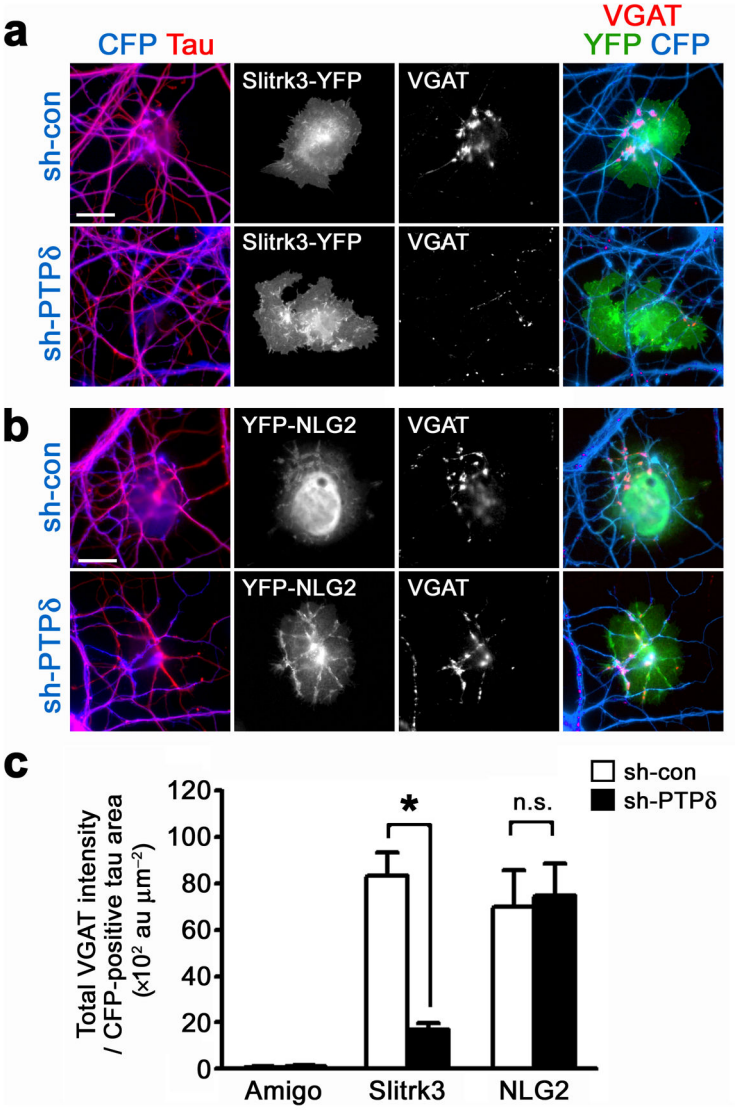

Figure 8. Slitrk3 requires PTPδ for induction of inhibitory presynaptic differentiation

(**a**,**b**) Cultured hippocampal neurons were transfected at 0 DIV by Amaxa nucleofectionwith a vector co-expressing ECFP and either control shRNA (sh-con) or shRNA against PTPδ (sh-PTPδ). The transfected neurons were cocultured at 14 DIV with COS cells expressing Amigo-YFP (images not shown), Slitrk3-YFP (**a**) or YFP-NLG2 (**b**), and immunostained for VGAT at 15 DIV. A majority of axons (labeled with dephosphorylated tau) were transfected with shRNA-expressing vectors. COS cells expressing Slitrk3 induced little VGAT clustering along contacting axons of PTPδ knockdown neurons compared to contacting axons of control neurons (**a**). In contrast, COS cells expressing NLG2 induced VGAT clustering along contacting axons of PTPδ knockdown neurons as well as those of control neurons (**b**).

(**c**) Total integrated intensity of VGAT staining on CFP-positive axons associated with COS cells expressing Amigo, Slitrk3 or NLG2 and not associated with MAP2 (images not shown) divided by the CFP-positive axon contact area. Kruskal-Wallis ANOVA, $P < 0.0001$, $n = 30$,

40 and 30 cells for Amigo-YFP, Slitrk3-YFP and YFP-NLG2, respectively; *P< 0.001 compared with sh-con by Dunn's pairwise post-hoc test. n.s., not significant (P > 0.05). Data are presented as mean ± s.e.m. Scale bars represent 20 μm.